JOURNAL OF GEOPHYSICAL RESEARCH, VOL. 117, B09303, doi:10.1029/2012JB009302, 2012

Using repeated sources to quantitatively determine temporal change of medium properties: Theory and an example

Hui Long[1] and Lianxing Wen[1,2]

Received 12 March 2012; revised 16 July 2012; accepted 19 July 2012; published 5 September 2012.

[1] We develop a theory of using difference wavefields of repeated sources to locate and quantify temporal medium change and apply the theory to locate temporal change of seismic properties beneath the Japan subduction zone using repeated earthquakes. Our theory states the difference wavefields of two repeated sources in a temporally changed medium can be equivalently treated as wavefields propagating from conceptual sources, with their location at the place of temporal change and their strengths equal to the product of magnitude of medium property change and magnitude of the initial wavefields from the repeated sources. When the medium change extends to a finite region, the conceptual sources become volumetric sources distributed over the region of the medium change and propagating in the direction of the initial wave. The conceptualization establishes a theoretical framework for possible applications of using difference wavefields to locate and quantify temporal medium changes in geological sciences, ultrasonic experiments, civil engineering and medical imaging. We search repeating earthquakes occurring in the Japan subduction zone, formulate an empirical procedure to extract the difference wavefields between repeating earthquakes and determine temporal change of seismic properties using a back-projection method. We locate the temporal change of seismic properties beneath the Japan subduction zone to be at (37.2°N, 142°E), and estimate the magnitude of the conceptual body force associated with the temporal change to be 1.15×10^{10}N, or as a reference, a 0.87% density change for an assumed volume of temporal change of 10^3 km^3.

Citation: Long, H., and L. Wen (2012), Using repeated sources to quantitatively determine temporal change of medium properties: Theory and an example, *J. Geophys. Res.*, *117*, B09303, doi:10.1029/2012JB009302.

1. Introduction

[2] Using seismic or ultrasonic waves to probe temporal change in the medium is an important topic in ultrasound experiments, civil engineering, medical imaging and geological sciences. In ultrasound experiments, scattered waves of repeated sources are used to estimate nonlinear behavior in seismic velocity using coda wave interferometry [*Snieder et al.*, 2002; *Grêt et al.*, 2006]. In civil engineering, repeated ultrasonic waves are used to monitor rock fractures of a building [*Young and Collins*, 2001]. In medical imaging, ultrasound images have been used to monitor cerebral blood flow changes in focal ischemia in rabbits [*Els et al.*, 1999; *Bonnin et al.*, 2008; *Li et al.*, 2010]. And, in geological sciences, repeated seismic sources or explosions are used to monitor volcano activities [*Poupinet et al.*, 1984; *Martini et al.*, 2009], seismic velocity changes before an earthquake [*Niu et al.*, 2008] and following large earthquakes [*Li et al.*, 1998; *Baisch and Bokelmann*, 2001; *Matsumoto et al.*, 2001; *Vidale and Li*, 2003; *Ikuta and Yamaoka*, 2004; *Schaff and Beroza*, 2004; *Nishimura et al.*, 2005; *Peng and Ben-Zion*, 2006; *Rubinstein et al.*, 2007; *Li et al.*, 2007; *Cheng et al.*, 2011], temporal evolution of oil production fields [*Lumley*, 2001; *Rickett and Lumley*, 2001], underground carbon sequestration [*Santos and Harris*, 2009] and temporal change of seismic signals related to change of the properties in the crust [*Bokelmann and Harjes*, 2000; *Furumoto et al.*, 2001; *Niu et al.*, 2003; *Taira et al.*, 2008; *Zhao and Peng*, 2009; *Cheng et al.*, 2011] and in the Earth's core [*Zhang et al.*, 2005; *Wen*, 2006; *Cao et al.*, 2007; *Zhang et al.*, 2008]. Recently, repeated ambient noise analysis provides another means for monitoring temporal change of elastic medium [*Sens-Schönfelder and Wegler*, 2006; *Snieder et al.*, 2007; *Wegler and Sens-Schönfelder*, 2007; *Brenguier et al.*, 2008a, 2008b].

[3] It is clear from these studies that probing temporal medium change has not only started to provide fundamental insights into physics of many geophysical phenomena, such as

[1]Department of Geosciences, State University of New York at Stony Brook, Stony Brook, New York, USA.

[2]School of Earth and Space Sciences, University of Science and Technology of China, Hefei, China.

Corresponding author: H. Long, Department of Geosciences, State University of New York at Stony Brook, Stony Brook, NY 11794, USA. (hulong@ic.sunysb.edu)

©2012. American Geophysical Union. All Rights Reserved.
0148-0227/12/2012JB009302

earthquake nucleation, fault zone damage and healing process, volcano activities, stress build-up in the crust and the thermo-chemical processes in the top of the Earth's inner core, but also become a practical and effective tool for monitoring evolution of oil fields and underground carbon sequestration. Two types of approach have been developed in detecting temporal change of medium properties. One approach is to obtain the medium images at different time steps and extract the difference between the images, while the other one is to relate the difference of waveform characteristics of the repeated sources or the Green's functions obtained from noise correlations to temporal change of medium properties. The issue, however, has always been challenging, because the signal associated with the temporal change is usually very weak compared to background waves, and the methods of detecting it require extremely high resolution and great care. In the approach of comparing images at different time steps, the presence of noise and actual station distribution make the resolution analysis difficult in constructing images using the background waves. The potential artifacts in the time-lapse images could significantly affect the identification and inference of temporal change in the medium. In the approach of relating the difference of waveform characteristics of the repeated sources or the Green's functions obtained from noise correlations to temporal change of medium properties, the repeatability of the source is always a practical issue for both ambient noise and repeated events including the controlled sources. In addition, most of the methods in this approach only provide an average estimation of the bulk medium.

[4] In this paper, we establish a theoretical framework that conceptualizes propagation of difference waves fields, defined as the wavefield difference between the repeated sources, and uses difference wavefields to effectively image temporal change of properties in the medium. The conceptualization we propose would make experiment design and resolution analysis straightforward, and overcome many challenging issues in the current methods of determining temporal property change in the medium. The conceptualization also makes it possible to pinpoint and quantify temporal change inside the medium. We apply the theory to search temporal change of medium properties beneath the Japan subduction zone using the difference *SH* waveforms of a pair of moderate-size earthquake doublet recorded at the Hi-net stations. We present the theory in Section 2, application to the determination of temporal seismic change beneath the Japan subduction zone in Section 3, and discussion and conclusion in Sections 4, 5.

2. Theoretical Framework of Relating the Difference Wavefields With Temporal Change of Medium

[5] We use two-dimensional *SH* wave propagation to demonstrate the concept. The extension of the concept to the *P-SV* system or to three-dimensional wave propagation is straightforward. We are dealing with the wave propagation problem that repeated sources are used at (x_s, z_s), and there is a change of medium properties of density and shear modulus between the timing of the repeated sources. The theory is to relate the observed difference wavefields to the location and magnitude of the property changes in the medium.

[6] *SH* elastic wave propagation in a two-dimensional *x-z* medium is governed by the following equations:

$$-f\delta(x-x_s, z-z_s) + \rho(x,z)\frac{\partial v}{\partial t} = \frac{\partial \sigma_{xy}}{\partial x} + \frac{\partial \sigma_{zy}}{\partial z} \quad (1)$$

$$\frac{\partial \sigma_{xy}}{\partial t} = \mu(x,z)\frac{\partial v}{\partial x} \quad (2)$$

$$\frac{\partial \sigma_{zy}}{\partial t} = \mu(x,z)\frac{\partial v}{\partial z} \quad (3)$$

where f is body force, (x_s, z_s) location of repeated sources, v velocity wavefield, σ_{xy}, σ_{zy} stresses, ρ density, μ shear modulus, and t time.

[7] Let $v = v_0$, $\sigma_{xy} = \sigma_{xy,0}$, $\sigma_{zy} = \sigma_{zy,0}$ be the velocity and stress wavefields and $\rho = \rho_0$, $\mu = \mu_0$ the density and shear modulus of the medium associated with the first source; $v = v_0 + \delta v$, $\sigma_{xy} = \sigma_{xy,0} + \delta\sigma_{xy}$, $\sigma_{zy} = \sigma_{zy,0} + \delta\sigma_{zy}$, $\rho = \rho_0 + \delta\rho$, $\mu = \mu_0 + \delta\mu$ be those of the latter source. Inserting these variables for the latter source into equations (1)–(3) and ignoring second-order perturbations, one yields the following equations related to the difference wavefields:

$$\rho(x,z)\frac{\partial \delta v}{\partial t} + \delta\rho(x,z)\frac{\partial v_0}{\partial t} = \frac{\partial \delta\sigma_{xy}}{\partial x} + \frac{\partial \delta\sigma_{zy}}{\partial z} \quad (4)$$

$$\frac{\partial \delta\sigma_{xy}}{\partial t} = \mu(x,z)\frac{\partial \delta v}{\partial x} + \delta\mu(x,z)\frac{\partial v_0}{\partial x} \quad (5)$$

$$\frac{\partial \delta\sigma_{zy}}{\partial t} = \mu(x,z)\frac{\partial \delta v}{\partial z} + \delta\mu(x,z)\frac{\partial v_o}{\partial z} \quad (6)$$

where $\delta\rho$, $\delta\mu$ are temporal change of density and shear modulus between the sources, and δv, $\delta\sigma_{xy}$, $\delta\sigma_{zy}$ are difference velocity and stresses of the wavefields as a result of the medium property changes.

[8] Let us first consider the case that the property change is localized at a single point in space(x_c, z_c), i.e., $\delta\rho(x, z) = \Delta\rho\delta(x - x_c, z - z_c)$ and $\delta\mu(x, z) = \Delta\mu\delta(x - x_c, z - z_c)$. Equations (4)–(6) now become:

$$\rho(x,z)\frac{\partial \delta v}{\partial t} - f\delta(x-x_c, z-z_c) = \frac{\partial \delta\sigma_{xy}}{\partial x} + \frac{\partial \delta\sigma_{zy}}{\partial z} \quad (7)$$

$$\frac{\partial \delta\sigma_{xy}}{\partial t} = \mu(x,z)\frac{\partial \delta v}{\partial x} + s_x\delta(x-x_c, z-z_c) \quad (8)$$

$$\frac{\partial \delta\sigma_{zy}}{\partial t} = \mu(x,z)\frac{\partial \delta v}{\partial z} + s_z\delta(x-x_c, z-z_c) \quad (9)$$

where $f = -\Delta\rho\frac{\partial v_0}{\partial t}\big|_{(x,z)=(x_c,z_c)}$, $s_x = \Delta\mu\frac{\partial v_0}{\partial x}\big|_{(x,z)=(x_c,z_c)}$, and $s_z = \Delta\mu\frac{\partial v_0}{\partial z}\big|_{(x,z)=(x_c,z_c)}$.

[9] Note that, other than two additional source terms, s_x and s_z being at (x_c, z_c), and the body force term f at (x_c, z_c), equations (7)–(9) are identical to equations (1)–(3). Equations (7)–(9) thus state that the difference wavefields can be treated as the wavefields that propagate in the same medium as the initial waves, with a conceptual body force f and conceptual stress perturbations, s_x and s_z, at the

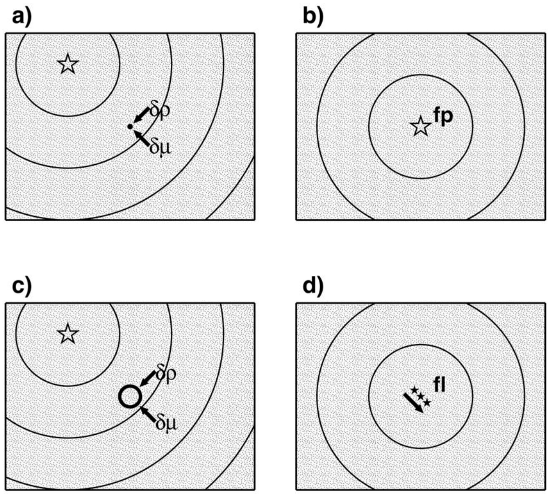

Figure 1. Conceptualization of propagation of difference wavefields of repeated sources in changed media. (a) Cartoon illustration of wave propagation of repeated sources in a temporally changing medium. Sources are repeated at the location represented by star. Between the repeated sources, a density change ($\delta\rho$) and a shear modulus change ($\delta\mu$) occur at the location represented by dot; (b) conceptual source model for propagation of difference wavefields in Figure 1a. Wavefields propagate in the same background medium in Figure 1a, the conceptual source situates at the location where the medium change occur (star and dot in a); and the strength of the conceptual source, *fp*, is a summation of s_x, s_z, and f (see text); (c) same as Figure 1a, except that the medium changes extend to a finite region represented by circle; (d) volumetric sources model for propagation of difference wavefields in Figure 1c. Wavefields propagate in the same background medium in Figure 1c, volumetric sources (stars in a circular volume lined up in the propagating direction of source) are distributed in the region of medium changes and propagating in the direction of initial wave (arrow), the strength of the net force, *fl*, is the volumetric integration of *fp* in Figure 1b.

location of property change (Figures 1a and 1b). The magnitude of the conceptual body force is equal to the negative of the product of density change and acceleration of the initial wavefields at the location of density change; the magnitudes of the conceptual stress perturbations are equal to the product of shear modulus change and strains (displacement gradients) of the initial wavefields at the location of shear modulus change.

[10] When temporal change of elastic properties extends to a finite region, the conceptual source would be the volumetric integration of equivalent forces in the region of medium change. Since the initial wavefields (acceleration and strains) of the actual source arrive at different time for different parts of the changed medium and the equivalent forces take effects at the arrival times of the initial waves, the equivalent forces become a propagating force, traveling in the direction of initial waves impinged on the changed medium (Figures 1c and 1d).

[11] Numerical simulations indicate that such conceptualization of difference wave propagation accurately reproduces the difference wavefields. An example is shown for a homogeneous whole space medium (Figures 2a–2d). In this example, the earlier source generates a wavefield in a homogeneous whole space and the latter source propagates through the same medium, but with a density change of 50% at the point represent by the dot (Figure 2a). The wavefields for the two sources are calculated by a finite difference technique [*Wen*, 2002] and difference wavefields are obtained

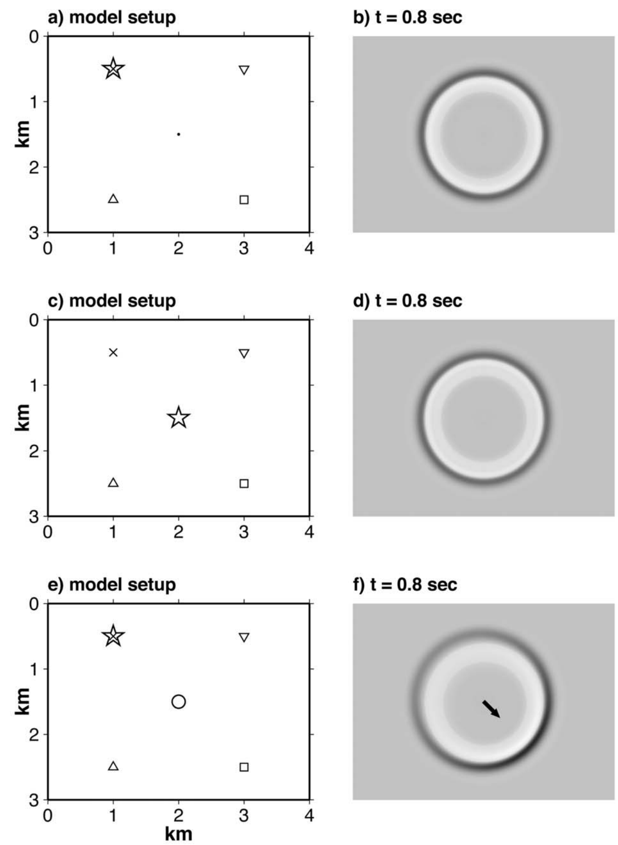

Figure 2. Comparisons of difference wavefields of repeated sources from a conceptual source for a homogeneous whole space with a density of 2.6 g/cm^3 and a shear velocity of 2.85 km/s. (a) model setup, repeated sources (star) and location of the density change (dot); (b) a snapshot of difference wavefields of the repeated sources. Difference wavefields are obtained by subtracting the wavefields for homogeneous whole space from those for a model with a density change of 50% in the location represented by the dot in whole space; (c) model setup for wavefields of a conceptual source located at the place of density change (star and the same represented by dot in Figure 2a, with a strength equal to the product of density change and acceleration of the initial waves; (d) snapshot of wavefields for the conceptual source at the same time step in Figure 2b; (e) model setup same as in Figure 2a, except the density change occurs in a finite region represented by circles; (f) snapshot of difference wavefields for model e. For comparison, the amplitudes of residual fields are scaled to a point source based on the volumetric distribution of the density change. Arrow indicated the direction of the initial waves from the repeated sources impinged on the location of density change. Cross, triangles and square in three models represent four receiver sites.

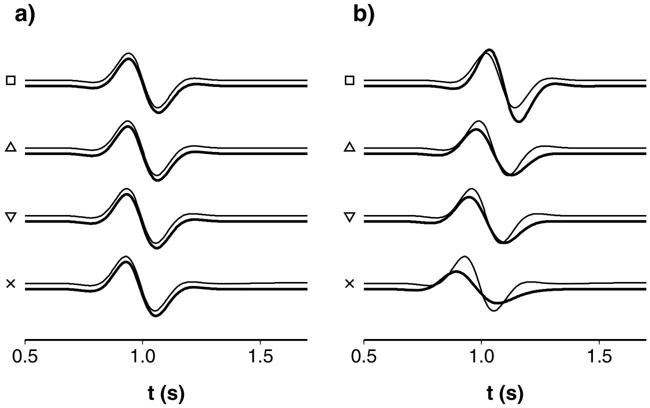

Figure 3. Synthetic waveform comparisons of difference wavefields of repeated sources from a conceptual source. (a) Comparisons of waveforms of difference wavefields (heavy traces) obtained for model setup in Figure 2a and wavefields (light traces) generated by a conceptual source for model setup in Figure 2c; (b) same as Figure 3a, except that wavefields are for model setup in Figure 2e. For comparison, the amplitudes of the residual fields are scaled based on the volumetric distribution of the density change. Synthetic waveforms are labeled with the symbols according to the receiver locations in Figures 2a, 2c, and 2e.

by subtracting the wavefields of the earlier source from those of the latter source (Figure 2b). In the conceptual model, a source is placed at the location of density change with the magnitude of the body force equal to the product of density change and acceleration of wavefields of the earlier source at the location of the density change (star, Figure 2c). The wavefields for the conceptual source model match the difference wavefields well in time, amplitude and shape. This is evident from snapshots (Figures 2b and 2d) and examples of waveform comparison (Figure 3a).

[12] When the density change extends to a finite region (Figure 2e), the residual wavefields exhibit direction dependence with respect to the direction of the initial waves from the repeated sources (Figure 2f), or directivity typical of a finite propagating source. The residual wavefields exhibit narrower shapes and stronger amplitudes (Figure 2f and the top traces in Figure 3b) in the direction of the initial wave impinged on the changed media (arrow in Figure 2f), broader shapes and smaller amplitudes (Figure 2f and the bottom traces in Figure 3b) in the direction away from the initial wave propagation, and waveform features intermediate to those in and away from the initial wave propagation (Figure 2f and the middle two trace pairs in Figure 3b) for the receivers in the direction perpendicular to the initial wave propagation.

[13] Since, except for the equivalent source terms, equations (7)–(9) are identical to the governing equations for the initial waves, the conceptualization of residual wavefields propagation (Figure 1) applies to any types of heterogeneous media. This is illustrated in a half-space model that consists of a free surface and random variations of seismic velocity of 4% with correlation scale lengths of 200 m in both x- and z- directions. The conceptual source in this case contains two major parts related to the initial direct wave and the reflected initial wave from the free surface, and minor components associated with the scattering of the initial waves from the random medium. The conceptual source model of wave propagation reproduces all the features of the residual waves, including various components related to direct, reflected and scattered initial waves, their interaction with free surface and interference of various components of residual waves, as evident from comparisons of snapshots (Figures 4b–4d and 4f–4h) and synthetic waveforms (Figure 5).

3. Application to Study Temporal Change of Seismic Properties Beneath the Japan Subduction Zone Using Earthquake Doublet

[14] As an example, we apply the theory to search and determine temporal change of seismic properties beneath the Japan subducution zone. Temporal seismic velocity changes are reported in the region associated with faulting and volcanic activities [*Furumoto et al.*, 2001; *Matsumoto et al.*, 2001; *Nishimura et al.*, 2005; *Rubinstein et al.*, 2007] and the region is covered by more than 700 high-resolution Hi-Net seismic stations. We will rely on earthquake doublets as sources. In the following subsections, we present doublet search, an empirical procedure for the extraction of the difference wavefields and results of inferred temporal change of seismic properties in the region.

3.1. Doublet Search

[15] We adopt the procedures outlined in [*Yu and Wen*, 2012] to search possible doublets in the Japan subduction zone. We briefly review the procedures here. We first group event-pairs based on the event catalog between 2004 and 2010 provided by the Incorporated Research Institutions for Seismology for events that are less than 40 km away and with a body wave magnitude larger than 4.0. We collect vertical component data for those event-pairs from the seismic stations at the Global Seismographic Network (GSN), and band-pass filter the data from 0.8 to 1.5 Hz. Waveforms are further selected based on high signal-to-noise ratios. We cross-correlate the waveforms recorded at each GSN station between possible event-pairs. Highly similar neighboring events with an average cross-correlation coefficient higher than 0.95 are selected for further event relocation.

[16] We use the most similar and closest doublet located on the eastern coastline of Japan as repeated sources (Figure 6c). The doublet consists of two events occurring in 2005 and 2009 (Table 1). The GSN recordings of this doublet constitute good azimuthal coverage for determining their relative location (Figures 6a and 6c). We employ a master event relocation method developed by *Wen* [2006] to relocate the doublet. Relative location of the doublet is determined by minimizing the RMS travel time residuals of the P or Pn phase observed at GSN stations [*Wen*, 2006]. The relocation procedures place the 2009 event 225 m east and 40 m north to the 2005 event (Figures 6b and 6d).

3.2. Extraction of Difference Wavefield

[17] In extracting the difference wavefields resulted from the temporal change of medium, the source difference of the repeated sources has always been a challenging issue in both passive and active source experiments. To minimize the effects of source difference between the 2005 and 2009

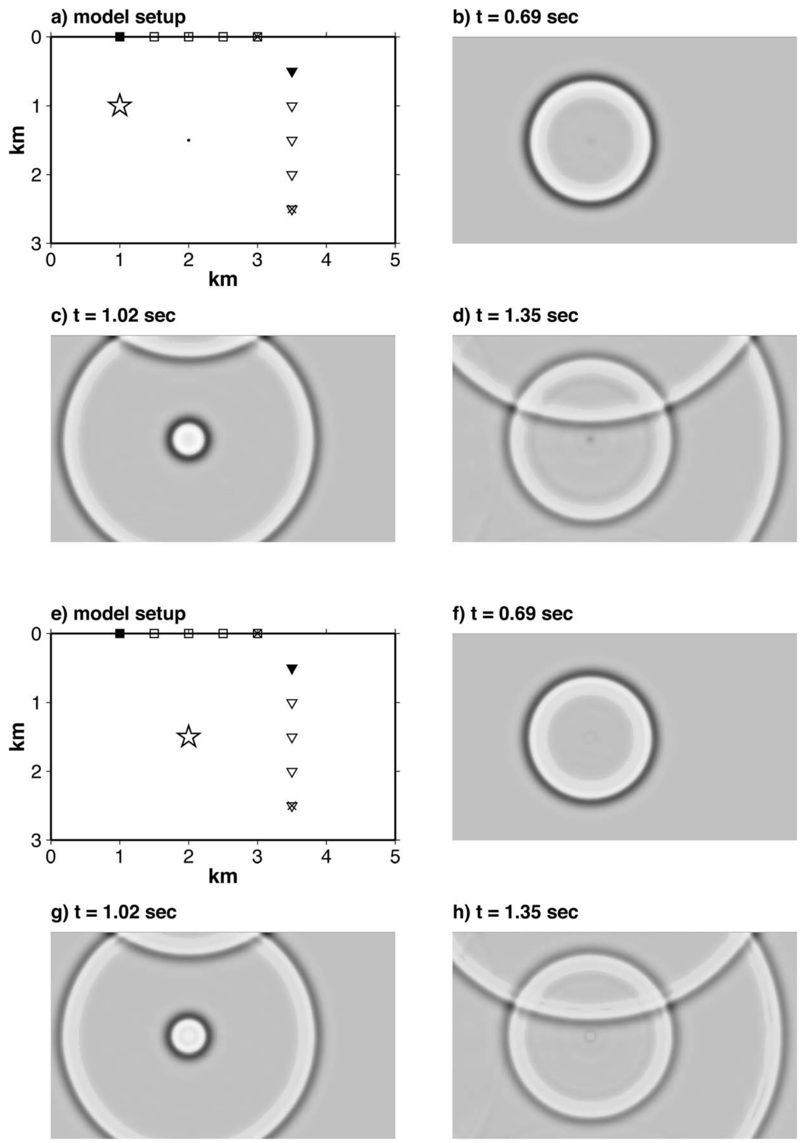

Figure 4. Comparisons of residual wavefields of repeated sources and wavefields from a conceptual source for a half-space model with a density of 2.6 g/cm^3, a shear velocity of 2.85 km/s and random velocity variations of 4% with correlation lengths of 200 m in both horizontal and vertical directions. (a) Model setup, repeated sources (star), location of density change (dot); the magnitude of density change is 50% between the repeated sources; (b–d) snapshots of residual wavefields of the repeated sources; (e) model setup for wavefields of a conceptual source situated at the location of density change (star, and the same represented by dot in Figure 4a, with a strength equal to the product of density change and acceleration of the initial waves; (f–h) snapshots of wavefields for the conceptual source at the same time steps in Figures 4b–4d. Squares and triangles in Figures 4a and 4e indicate receiver locations where synthetic waveforms of two wavefields are shown in Figure 5.

doublet, two steps are adopted in the extraction of difference wavefields for each station between the two events. We use the observations recorded at a Hi-Net station MTDH (red triangle in Figure 9) as an example to illustrate the procedures (Figure 7).

[18] Because we are dealing with the *SH* wave propagation, we only use the transverse components of the seismic data. We first align the waveforms of the doublet by cross-correlation and normalize the waveforms (Figures 7a and 7e). The normalization procedure is based on one event as a reference, and uses the ratio of 20-s waveform integration between the doublet to correct for amplitude difference of the other event due to the magnitude difference between the doublet at each station. We then extract difference wavefields between the doublet by weighting the subtraction of the normalized waveforms based on the cross-correlation coefficient between the doublet waveforms (Figures 7b–7d and 7f–7h). In this step, we calculate cross-correlation coefficient between the doublet waveforms within a 2-s time window and move the cross-correlation time window every

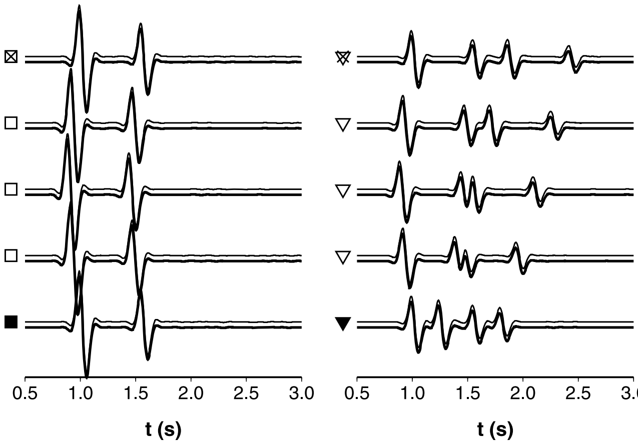

Figure 5. Comparisons of waveforms of difference wavefields (heavy traces) obtained for model setup in Figure 4a and wavefields (light traces) generated for a conceptual source for model setup in Figure 4e. Synthetic waveforms are labeled with symbols according to the receiver locations in Figures 4a and 4e.

0.1 s through the time series (Figures 7d and 7h). Waveform subtraction is weighted by a binary function of a value of zero for the time windows with a cross-correlation coefficient greater than a cut-off value and a value of one for other windows (Figures 7c, 7d, 7g, and 7h). In another word, we only regard the difference waveforms in the de-correlated time windows (with the correlation coefficient lower than the cut-off value) as the signals resulted from temporal change of media. The difference waveforms in the correlated time windows (with correlation coefficient higher than the cut-off value) are regarded as the results from the slight differences in source radiation between the doublet. The cross-correlation coefficients are high in most of the time windows, but decrease dramatically at some time windows (Figure 7d). A cut-off value of 0.93 is chosen empirically in this example.

[19] After these two steps, we exclude stations with the amplitude of the extracted difference wavefield signal smaller than the level of the background noise, defined as the amplitude of the waveform difference of the doublet before the Pn wave. To further ensure the quality of the data, we only use those waveforms with average cross-correlation coefficient larger than 0.98 for imaging temporal medium change. Of about 700 stations in the Hi-Net, a total of 36 stations are selected based on the these selection criteria, with 19 stations on the southwest side, 9 stations on the west side and 8 stations on the northwest side (triangles, Figure 9). The seismic data and extracted signals at these stations have been further eye-checked for their waveform qualities (Figure 8). The station distribution indicates such signals are observable at large area.

3.3. Determination of Temporal Change of Seismic Properties

[20] We use the observed difference *SH* wavefields to locate and quantify temporal change of seismic properties between the occurring times of the doublet. We determine the location of the temporal medium change based on the arriving times of the extracted difference signal and the magnitude of the temporal change based on the amplitudes of extracted signal and the acceleration of initial wavefields at the determined location of temporal medium change.

[21] The conceptualization theory states that the arriving time of the signal caused by the temporal change of seismic properties at each station is the summation of the travel time from the repeated events to the location of temporal changes (the conceptual sources) and the travel time from the conceptual sources to the station. Therefore, for a signal detected at a station, the possible conceptual sources locate at one ellipsoid-shaped surface based on the arrival time of the signal. When we have multiple stations, we can determine the location of the conceptual source, which is where those ellipsoid surfaces overlay. This back projection is implemented in the following steps, similar to those used to determine seismic scatterers in the deep mantle from PKP precursors [*Wen*, 2000; *Niu and Wen*, 2001]. For each station, we first determine its ellipsoid surface based on the station location, event location and the arrival time of the extract difference wavefields. We then assign the relative energy of the extracted difference wavefields (with respect to the maximum of the background field) to the grids of the ellipsoid surface. When multiple stations are used and their ellipsoid surfaces overlay, the projected energy is averaged. These projection steps are repeated for each assumed depth of the temporal change.

[22] We use Preliminary Reference Earth Model (PREM) [*Dziewonski and Anderson*, 1981] to calculate the travel times and adopt a grid size of 0.2 by 0.2 degree based on the errors in predicting the Sn arrival times by PREM. The back-projection procedure places the location of temporal change at (37.2°N, 142°E), where the projected energy of the difference wavefields is focused. The energy of the difference wavefields is about 3.5% relative to the main energy of the observations. Forward calculation indicates that the predicted difference wavefields travel times based on the inferred position of the temporal change are consistent with either the first or the secondary arrivals of the extracted difference wavefield at those stations. Given the uncertainties of the model in predicting Sn arrival times, the uncertainty in the depth determination of the temporal change is large, between 0 and 80 km. If we assume that the temporal changes occur at the slab interface, they should be located at 35 km depth based on the slab depth contours in the region (Figure 9).

[23] While the relative amplitudes are projected back to determine the location of temporal change, the absolute amplitude of the observed difference wavefields are used to estimate the magnitude of medium property change. The displacement generated by a single force can be expressed by:

$$U_i(\vec{x}, t) = \frac{1}{4\pi\rho v^2 r}\left(\delta_{ij} - \frac{\partial r}{\partial x_i}\frac{\partial r}{\partial x_j}\right)F_j\left(t - \frac{r}{v}\right) \tag{10}$$

where U_i is displacement in i direction, F_j body force in j direction, v velocity and r distance from the source to the receiver [*Aki and Richards*, 2002]. For each station, we know the amplitude of difference wavefields, and the distance from the conceptual source to the station, r, so we can estimate the magnitude of the body force, F_j. When multiple

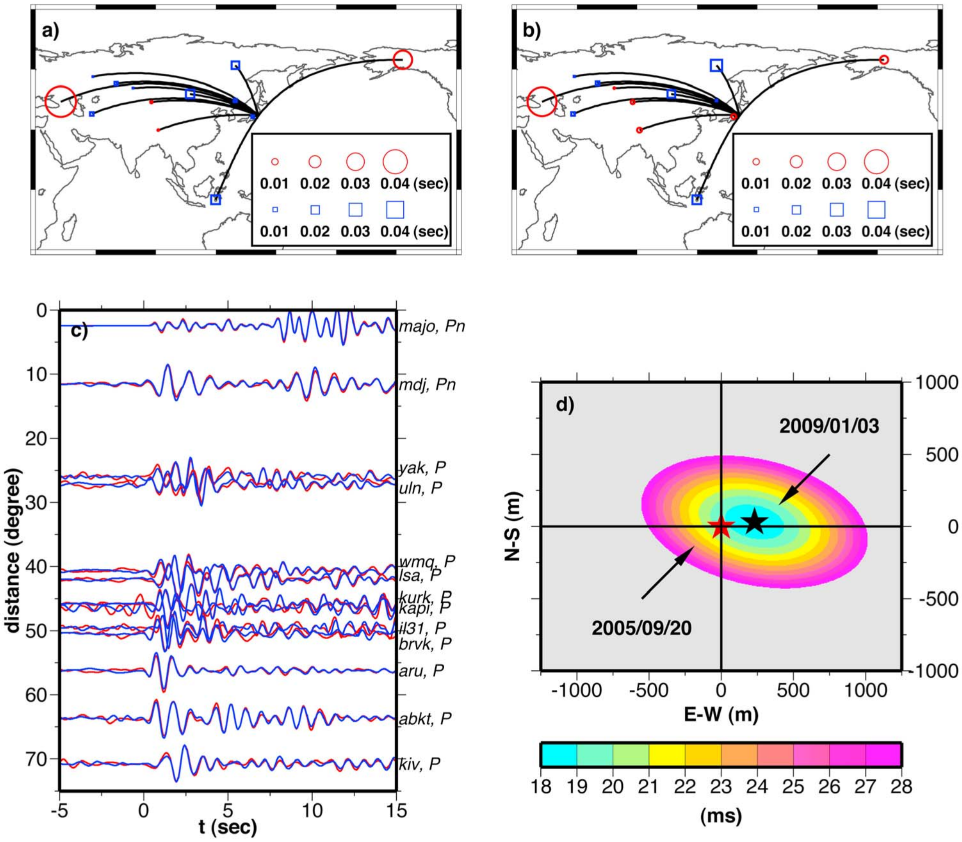

Figure 6. Relocation results of the 2005/09/10 and 2009/01/03 doublet. (a) Measured difference in absolute arrival time (circles and squares) of P, Pn arrivals between two events, plotted centered at the location of each station, along with the great circle paths (black traces) from source to station. The arrival time differences are plotted with respect to a source origin time difference that generates a zero mean of the travel time differences for all stations. Red circles indicate that the P or Pn phase in the 2005 event arrives relatively later than in the 2009 event, while blue squares show the opposite (scale shown in the inset in the unit of sec). (b) Travel time residuals between the two events after corrections using the best fitting relative location and origin time for the 2005 event. (c) Vertical components of waveform of the two events recorded at GSN stations aligned along the P, Pn arrivals, waveforms are filtered with the worldwide standard seismic network short-period instrument response and labeled with station name and seismic phase used in the relocation. Red traces are waveforms from the 2005 event while blue traces from the 2009 event. (d) Best fitting location of the 2009 event (star) relative to the location of the 2005 event (circle) that minimizes the RMS travel time residual of the P, Pn phase observed at GSN stations shown in Figure 6c. The RMS residuals larger than 28 ms are plotted as background.

stations are used, the magnitude of body force F is the average. As from equation (7), the magnitude of the conceptual source per volume is $f = -\Delta\rho \frac{\partial v_0}{\partial t}\big|_{(x,z)=(x_c,z_c)}$, where $\Delta\rho$ is density change and $\frac{\partial v_0}{\partial t}\big|_{(x,z)=(x_c,z_c)}$ acceleration of the initial wavefields at the location of temporal change, and the equivalent body force $F = Vf$ with V representing the volume of the region of temporal change, the volumetric integral of density change can be estimated by equation:

$$\Delta\rho V = -F \Big/ \left(\frac{\partial v_0}{\partial t}\Big|_{(x,z)=(x_c,z_c)} \right). \tag{11}$$

Table 1. Doublet Information

Event	Date (year/mm/dd)	Origin Time (hh:mm:ss)	Latitude (°N)	Longitude (°E)	Magnitude (Mb)
2009 (master event)	2009/01/03	07:13:05.00	37.1270	141.0560	4.8
2005 (before relocation)	2005/09/10	20:06:50.00	37.0650	141.1850	4.7
2005 (after relocation)	2005/09/10	20:06:50.01	37.0654	141.1871	4.7

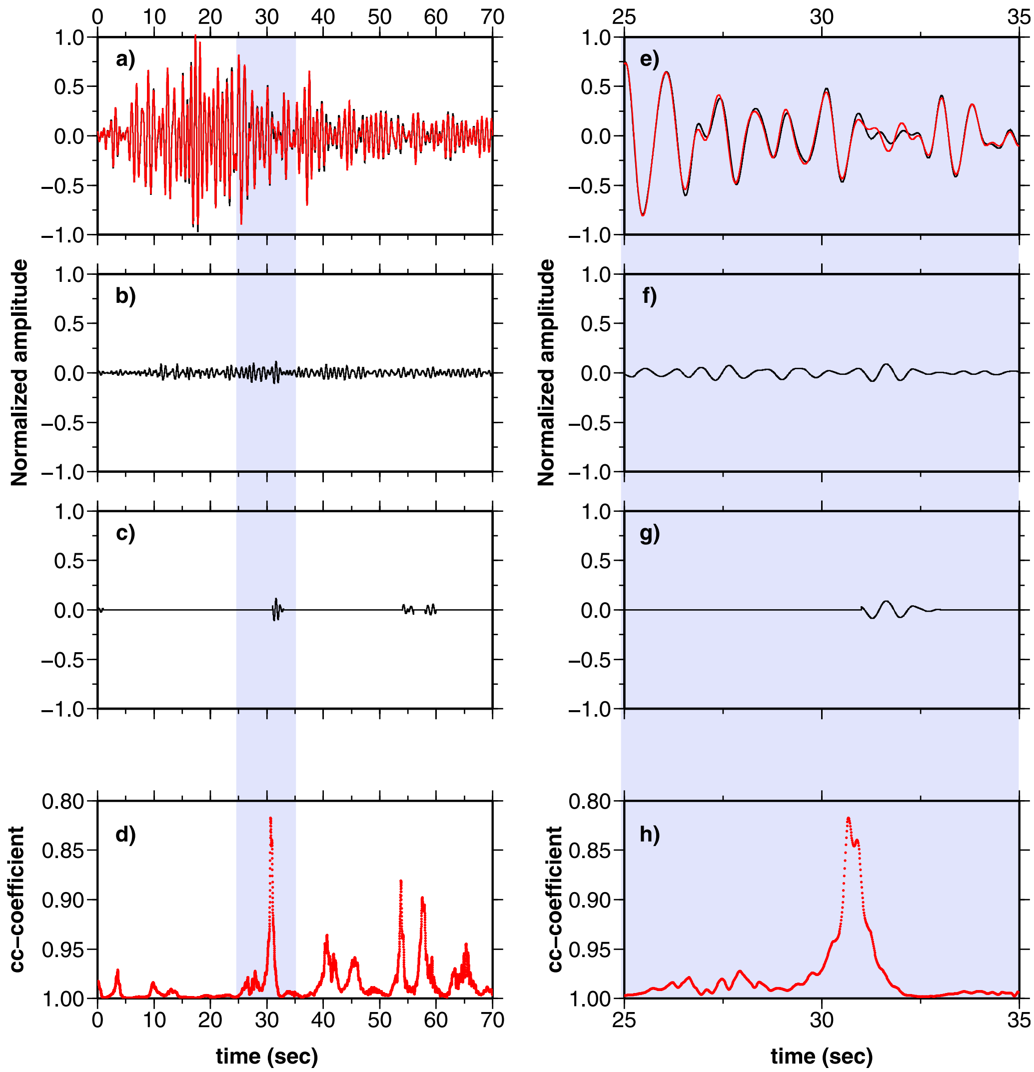

Figure 7. Procedures of extracting difference wavefields between the doublet, using station MTDH (noted red triangle in Figure 9) as an example. (a) Overlap of normalized waveforms of the doublet. Waveforms are aligned based on cross-correlation and amplitudes have been normalized. (b) Waveform difference obtained from the two waveforms shown in Figure 7a. (c) Waveform difference obtained based on a binary weighting function based on waveform cross-correlation values. (d) Cross-correlation coefficients between the two waveforms in Figure 7a. The moving time window for cross-correlation is 2 s, and the shifting time is 0.1 s. (e–h) Same as Figures 7a–7d, but for the time window between 25 s–35 s, the shaded regions in Figures 7a–7d.

[24] We estimate the acceleration of the initial waves of the 2005–2009 doublet based on the empirical relationship of the acceleration amplitudes with distance observed in the Hi-Net stations. The accelerations of the initial wavefields $\frac{\partial v_0}{\partial t}$ decay over distance (r) following this empirical relationship: $\frac{\partial v_0}{\partial t} = 2.1 \times 10^{-4} * r^{-2}$ m/s^2 based on the observations in the Hi-Net stations. Thus, based on the acceleration empirical relationship and the distance from the earthquake doublet to the location of temporal change, the acceleration at the location of the temporal change is estimated to be 3.2×10^{-4} m/s^2. The estimated magnitude of the conceptual body force associated with the temporal change of property is thus 1.15×10^{10}N. For reference, if we assume that the temporal change occurs within a volume of 10^3 km^3 and the density of oceanic crust to be 3.0 g/cm^3, the density change of the medium is estimated to be 0.87%.

[25] The detected temporal change of medium property between 2005 and 2009 is about 125 km away from the initiation of the 11 March 2011 Tohoku-Oki earthquake [*Chu et al.*, 2011] and within the rupture area of the earthquakes, as determined by many studies [*Ammon et al.*, 2011; *Ide et al.*, 2011; *Yue and Lay*, 2011] (Figure 8). The timing and location of the detected temporal change may provide insights on the initiation and rupture of the large earthquake.

4. Discussion

[26] Difference wavefields between earthquake doublets have been used to determine the temporal change of seismic

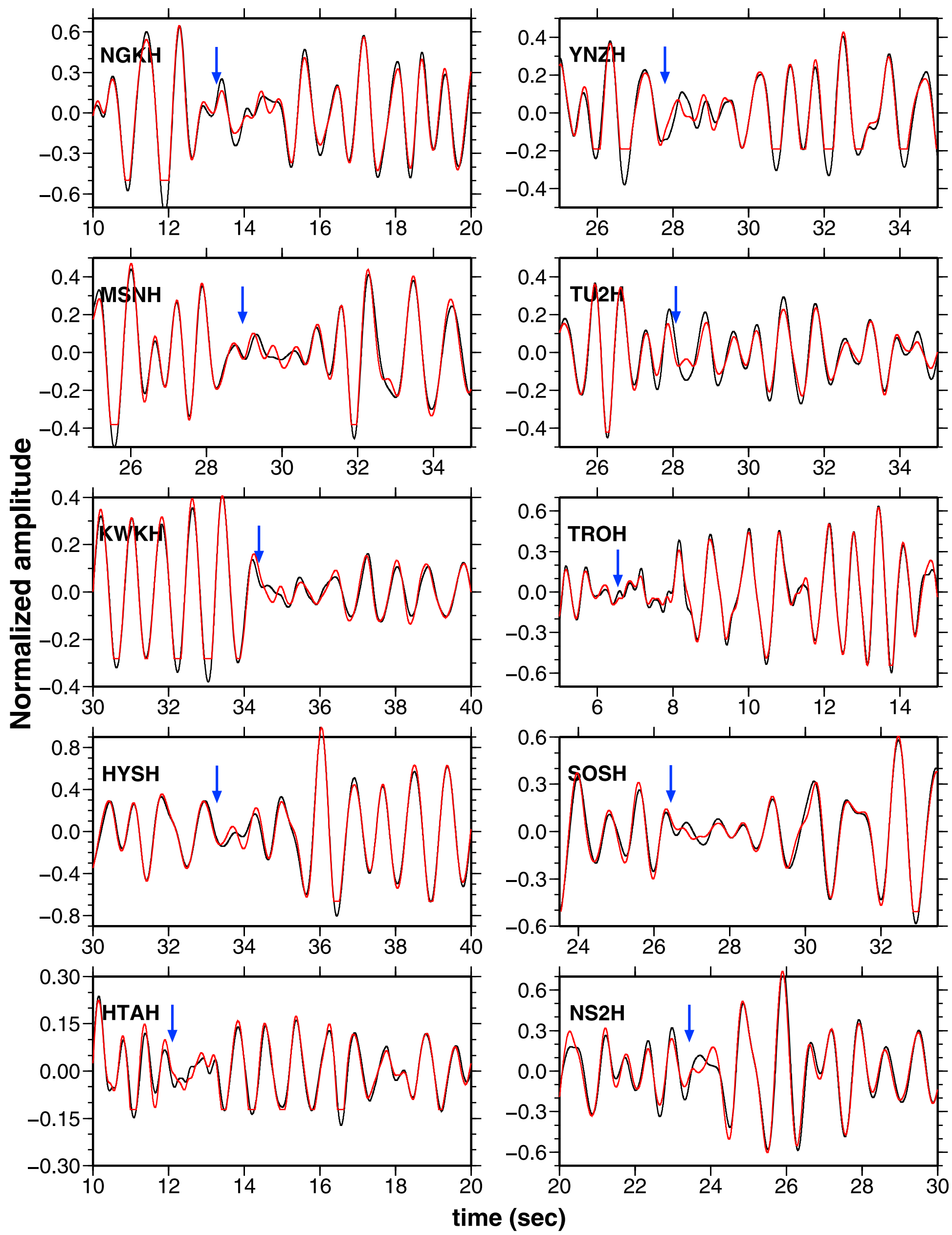

Figure 8. Overlap of normalized waveforms of the doublet recorded at other 10 stations (same as Figure 7e). Blue arrows mark the arrival times of the extracted difference wavefields signal for each station.

properties in the past [e.g., *Niu et al.*, 2003; *Taira et al.*, 2008; *Cheng et al.*, 2011]. There are similarities and differences between our study and the previous studies. In the previous studies, the difference wavefields were judged to be in existence based on cross-correlation coefficient between the doublet waveforms; the difference wavefields were projected back to possible locations of temporal changes based on their arrival times; and the length scale of the temporal change was determined based on the frequency of the difference wavefields and the length of the time window the difference waves existed. Our identification of difference wavefields and back projection procedure are very similar to theirs. However, unlike the previous studies, which were based on just an intuitive relationship between the difference wavefields and the temporal change of medium property, our study provides a theoretical framework relating the difference wavefields to the temporal change of seismic properties. Besides locating temporal changes, our theoretical framework also illustrates how different characteristics of difference wavefields are physically related to the temporal change of seismic properties and how can those characteristics be used to quantify temporal changes of seismic properties of the medium, including their location, magnitude, volume and type of medium property change.

[27] The doublet we used in this study has a source location separation of about 250 m. The difference wavefields we observed are unlikely due to the location difference between the doublet. A location difference of the doublet

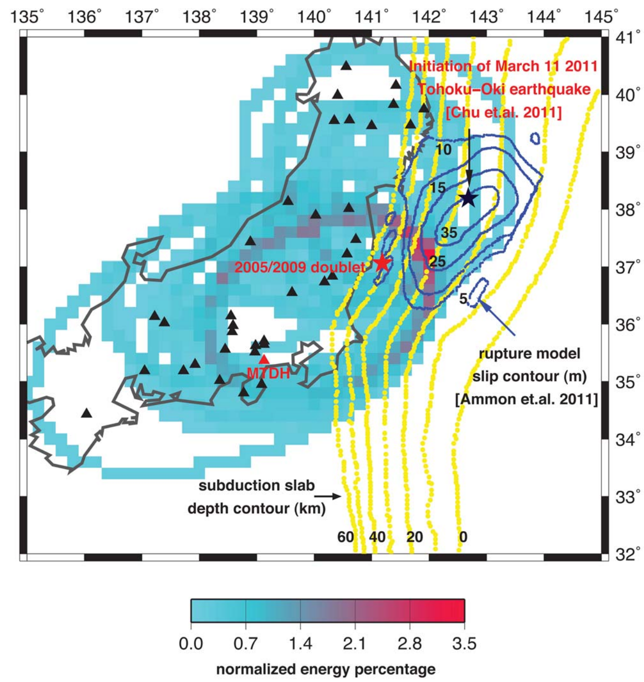

Figure 9. Back projected relative energy using a 0.2 degree by 0.2 degree grid size (see text for explanation). Black and red triangles represent Hi-net stations used for back projection. The projected energy is focused at (37.2°N, 142°E). Red and black stars represent the location of the 2005–2009 doublet and the initiation location of the March 11, 2011 Tohoku earthquake [*Chu et al.*, 2011], respectively. Yellow lines are reconstructed subducted slab depth contours from 0 to 60 km [*Nakajima and Hasegawa*, 2006; *Nakajima et al.*, 2009]. Blue lines are rupture slip contours of the March 11, 2011 Tohoku earthquake from *Ammon et al.* [2011].

will generate a decreased cross-correlation coefficient between the waveforms of the doublet, but such decrease is independent of time base on both theory and synthetics [*Snieder et al.*, 2002; *Snieder*, 2006; *Niu et al.*, 2003]. However, our observed quick decrease of cross-correlation coefficient is only isolated in a very limited time window (Figures 7d and 7h). The characteristics of the observed cross-correlation coefficients indicates that either the waveform difference due to the location difference is small or it does not arise in the time window our difference wavefields are extracted.

[28] The temporal changes of velocity and density are related to different types of conceptual sources and they are theoretically distinguishable based on their waveform characteristics and azimuthal variation. In our example, the complex propagation paths of the difference wavefields render it impossible to distinguish between the temporal changes of density and velocity, we have thus only considered the density change. Because of the station coverage, we are also unable to study the directivity of the difference wavefields in the data and cannot estimate the volume of the temporal change. It is hopeful that the seismic data of future simpler events or experiments in a controlled environment may be used to better constrain the volume of temporal change and separate the effects of temporal change of density from those of velocity.

5. Conclusions

[29] Using *SH* elastic wave propagation as an example, we derive a theory that conceptualizes the propagation of difference wavefields of repeated sources in a temporally changed medium. We show that the *SH* difference wavefields in the changed medium could be equivalently treated as wavefields propagating from a conceptual body source and two conceptual stress perturbations located at the place of temporal medium change, with the magnitude of the conceptual body force equal to the product of density change and acceleration of the initial wavefield at the location of density change, and the magnitudes of the conceptual stress perturbations equal to the product of shear modulus change and strains (displacement gradients) of the initial wavefields at the location of shear modulus change. When medium changes extend to a finite region, the conceptual sources become volumetric sources distributed over the region of the medium change and propagating in the direction of the initial wave.

[30] The conceptualization of propagation of difference wavefields of this study indicates that the problem of locating and quantifying temporal property changes in the medium can be essentially treated as a problem of locating and quantifying the strengths of the conceptual sources using difference wavefields. When the property changes extend to a finite region, the directivity of the difference wavefields can be used to further quantify the lateral extent of the conceptualized source, and thus, of the changed medium. The conceptualization overcomes many challenging issues in the current methods for determining temporal property changes in the medium. The conceptualization makes it possible to pinpoint and quantify exact location of temporal changes inside the medium and experiment design and resolution analysis for the detection of temporal medium change straightforward.

[31] As an example of application, we apply the theory to locate and quantify temporal change of seismic properties beneath the Japan subduction zone using an earthquake doublet as sources. We develop an empirical procedure to extract the *SH* component difference wavefields from the Hi-Net stations, which includes weighting the subtraction of the normalized waveforms between the doublet by a binary function based on cross-correlation coefficients between the waveforms. We detect temporal change of medium properties in the region and determine the location of the temporal change to be at (37.2°N, 142°E) based on the arrival times of the difference wavefields using a back-projection method. Based on the amplitudes of the extracted difference signal and the acceleration of the background wavefields, we estimate the magnitude of the conceptual body force associated with the temporal change is 1.15×10^{10}N, or, as a reference, a 0.87% density change, assuming that the temporal change occurs within a volume of 10^3 km^3. The detected temporal change of medium property between 2005 and 2009 is about 125 km away from the initiation of the 11 March 2011 Tohoku-Oki earthquake [*Chu et al.*, 2011] and within the rupture area of the earthquakes.

[32] **Acknowledgments.** We are grateful to IRIS, Hi-Net for providing the waveform data. This work is supported by NSF grants EAR-0911319 and EAR-1214215.

References

Aki, K., and P. G. Richards (2002), Elastic waves from a point dislocation source, in *Quantitative Seismology*, 2nd ed., edited by J. Ellis, pp. 63–117, Univ. Sci. Books, Sausalito, Calif.

Ammon, C. J., T. Lay, H. Kanamori, and M. Cleveland (2011), A rupture model of the great 2011 Tohoku earthquake, *Earth Planets Space*, *63*, 693–696, doi:10.5047/eps.2011.05.015.

Baisch, S., and G. H. R. Bokelmann (2001), Seismic waveform attributes before and after the Loma Prieta earthquake: Scattering change near the earthquake and temporal recovery, *J. Geophys. Res.*, *106*, 16,323–16,337, doi:10.1029/2001JB000151.

Bokelmann, G. H. R., and H. P. Harjes (2000), Evidence for temporal variation of seismic velocity within the upper continental crust, *J. Geophys. Res.*, *105*, 23,879–23,894, doi:10.1029/2000JB900207.

Bonnin, P., H. Debbabi, J. Mariani, C. Charriaut-Marlangue, and S. Renolleau (2008), Ultrasonic assessment of cerebral blood flow changes during ischemia-reperfusion in 7-day-old rats, *Ultrasound Med. Biol.*, *34*, 913–922, doi:10.1016/j.ultrasmedbio.2007.11.018.

Brenguier, F., N. M. Shapiro, M. Campillo, V. Ferrazzini, Z. Duputel, O. Coutant, and A. Nercessian (2008a), Towards forecasting volcanic eruptions using seismic noise, *Nat. Geosci.*, *1*, 126–130, doi:10.1038/ngeo104.

Brenguier, F., M. Campillo, C. Hadziioannou, N. M. Shapiro, R. M. Nadeau, and E. Larose (2008b), Postseismic relaxation along the San Andreas Fault at Parkfield from continuous seismological observations, *Science*, *321*, 1478–1481, doi:10.1126/science.1160943.

Cao, A., Y. Masson, and B. Romanowicz (2007), Short wavelength topography on the inner-core boundary, *Proc. Natl. Acad. Sci. U. S. A.*, *104*, 31–35, doi:10.1073/pnas.0609810104.

Cheng, X., F. Niu, P. G. Silver, and R. M. Nadeau (2011), Seismic imaging of scatterer migration associated with the 2004 Parkfield earthquake using waveform data of repeating earthquakes and active sources, *Bull. Seismol. Soc. Am.*, *101*, 1291–1301, doi:10.1785/0120100261.

Chu, R., S. Wei, D. V. Helmberger, Z. Zhan, L. Zhu, and H. Kanamori (2011), Initiation of the great Mw 9.0 Tohoku-Oki earthquake, *Earth Planet. Sci. Lett.*, *308*, 277–283, doi:10.1016/j.epsl.2011.06.031.

Dziewonski, A. M., and D. L. Anderson (1981), Preliminary reference Earth model, *Phys. Earth Planet. Inter.*, *25*, 297–356, doi:10.1016/0031-9201(81)90046-7.

Els, T., M. Daffertshofer, H. Schroeck, W. Kuschinsky, and H. Hennerici (1999), Comparison of transcranial Doppler flow velocity and cerebral blood flow during focal ischemia in rabbits, *Ultrasound Med. Biol.*, *25*, 933–938, doi:10.1016/S0301-5629(99)00049-6.

Furumoto, M., Y. Ichimori, N. Hayashi, Y. Hiramatsu, and T. Satoh (2001), Seismic wave velocity changes and stress build-up in the crust of the Kanto-Tokai region, *Geophys. Res. Lett.*, *28*, 3737–3740, doi:10.1029/2001GL013172.

Grêt, A., R. Snieder, and J. Scales (2006), Time-lapse monitoring of rock properties with coda wave interferometry, *J. Geophys. Res.*, *111*, B03305, doi:10.1029/2004JB003354.

Ide, S., A. Baltay, and G. C. Beroza (2011), Shallow dynamic overshoot and energetic deep rupture in the 2011 M(w) 9.0 Tohoku-Oki earthquake, *Science*, *332*, 1426–1429, doi:10.1126/science.1207020.

Ikuta, R., and K. Yamaoka (2004), Temporal variation in the shear wave anisotropy detected using the Accurately Controlled Routinely Operated Signal System (ACROSS), *J. Geophys. Res.*, *109*, B09305, doi:10.1029/2003JB002901.

Li, Y., J. E. Vidale, K. Aki, F. Xu, and T. Burdette (1998), Evidence of shallow fault zone strengthening after the 1992 M7.5 Landers, California, earthquake, *Science*, *279*, 217–219, doi:10.1126/science.279.5348.217.

Li, Y., P. Chen, E. S. Cochran, and J. E. Vidale (2007), Seismic velocity variations on the San Andreas fault caused by the 2004 M6 Parkfield earthquake and their implications, *Earth Planets Space*, *59*, 21–31.

Li, L., Z. Ke, K. Tong, and M. Ying (2010), Evaluation of cerebral blood flow changes in focal cerebral ischemia rats by using transcranial Doppler ultrasonography, *Ultrasound Med. Biol.*, *36*, 595–603, doi:10.1016/j.ultrasmedbio.2010.01.005.

Lumley, D. E. (2001), Time-lapse seismic reservoir monitoring, *Geophysics*, *66*, 50–53.

Martini, F., C. J. Bean, G. Saccorotti, F. Viveiros, and N. Wallenstein (2009), Seasonal cycles of seismic velocity variations detected using coda wave interferometry at Fogo volcano, Sao Miguel, Azores, during 2003–2004, *J. Volcanol. Geotherm. Res.*, *181*, 231–246, doi:10.1016/j.jvolgeores.2009.01.015.

Matsumoto, S., K. Obara, K. Yoshimoto, T. Saito, A. Ito, and A. Hasegawa (2001), Temporal change in P wave scatterer distribution associated with the M6.1 earthquake near Iwate volcano, northeastern Japan, *Geophys. J. Int.*, *145*, 48–58, doi:10.1111/j.1365-246X.2001.00339.x.

Nakajima, J., and A. Hasegawa (2006), Anomalous low-velocity zone and linear alignment of seismicity along it in the subducted Pacific slab beneath Kanto, Japan: Reactivation of subducted fracture zone?, *Geophys. Res. Lett.*, *33*, L16309, doi:10.1029/2006GL026773.

Nakajima, J., F. Hirose, and A. Hasegawa (2009), Seismotectonics beneath the Tokyo metropolitan area, Japan: Effect of slab-slab contact and overlap on seismicity, *J. Geophys. Res.*, *114*, B08309, doi:10.1029/2008JB006101.

Nishimura, T., S. Tanaka, T. Yamawaki, H. Yamamoto, T. Sano, M. Sato, H. Nakahara, N. Uchida, S. Hori, and H. Sato (2005), Temporal changes in seismic velocity of the crust around Iwate volcano, Japan, as inferred from analyses of repeated active seismic experiment data from 1998 to 2003, *Earth Planets Space*, *57*, 491–505.

Niu, F., and L. Wen (2001), Strong seismic scatterers near the core-mantle boundary west of Mexico, *Geophys. Res. Lett.*, *28*, 3557–3560, doi:10.1029/2001GL013270.

Niu, F., P. G. Silver, R. M. Nadeau, and T. V. McEvilly (2003), Stress-induced migration of seismic scatterers associated with the 1993 Parkfield aseismic transient event, *Nature*, *426*, 544–548, doi:10.1038/nature02151.

Niu, F., P. G. Silver, T. M. Daley, X. Cheng, and E. L. Majer (2008), Preseismic velocity changes observed from active source monitoring at the Parkfield SAFOD drill site, *Nature*, *454*, 204–208, doi:10.1038/nature07111.

Peng, Z. G., and Y. Ben-Zion (2006), Temporal changes of shallow seismic velocity around the Karadere-Duzce branch of the North anatolian fault and strong ground motion, *Pure Appl. Geophys.*, *163*, 567–600, doi:10.1007/s00024-005-0034-6.

Poupinet, G., W. L. Ellsworth, and J. Frechet (1984), Monitoring velocity variations in the crust using earthquake doublets: An application to the Calaveras Fault, California, *J. Geophys. Res.*, *89*, 5719–5731, doi:10.1029/JB089iB07p05719.

Rickett, J. E., and D. E. Lumley (2001), Cross-equalization data processing for time-lapse seismic reservoir monitoring: A case study from the Gulf of Mexico, *Geophysics*, *66*, 1015–1025.

Rubinstein, J. L., N. Uchida, and G. C. Beroza (2007), Seismic velocity reductions caused by the 2003 Tokachi-Oki earthquake, *J. Geophys. Res.*, *112*, B05315, doi:10.1029/2006JB004440.

Santos, E. T. F., and J. M. Harris (2009), DynaSIRT: A robust dynamic imaging method applied to CO_2 injection monitoring, *SEG Exp. Abstr.*, *28*, 4019, doi:10.1190/1.3255708.

Schaff, D. P., and G. C. Beroza (2004), Coseismic and postseismic velocity changes measured by repeating earthquakes, *J. Geophys. Res.*, *109*, B10302, doi:10.1029/2004JB003011.

Sens-Schönfelder, C., and U. Wegler (2006), Passive image interferometry and seasonal variations of seismic velocities at Merapi Volcano, Indonesia, *Geophys. Res. Lett.*, *33*, L21302, doi:10.1029/2006GL027797.

Snieder, R. (2006), The theory of coda wave interferometry, *Pure Appl. Geophys.*, *163*, 455–473, doi:10.1007/s00024-005-0026-6.

Snieder, R., A. Gret, H. Douma, and J. Scales (2002), Coda wave interferometry for estimating nonlinear behavior in seismic velocity, *Science*, *295*, 2253–2255, doi:10.1126/science.1070015.

Snieder, R., S. Hubbard, M. Haney, G. Bawden, P. Hatchell, A. Revil, and D. G. M. Working (2007), Advanced noninvasive geophysical monitoring techniques, *Annu. Rev. Earth Planet. Sci.*, *35*, 653–683, doi:10.1146/annurev.earth.35.092006.145050.

Taira, T., P. G. Silver, F. Niu, and R. M. Nadeau (2008), Detecting seismogenic stress evolution and constraining fault zone rheology in the San Andreas Fault following the 2004 Parkfield earthquake, *J. Geophys. Res.*, *113*, B03303, doi:10.1029/2007JB005151.

Vidale, J. E., and Y. Li (2003), Damage to the shallow Landers fault from the nearby Hector Mine earthquake, *Nature*, *421*, 524–526, doi:10.1038/nature01354.

Wegler, U., and C. Sens-Schönfelder (2007), Fault zone monitoring with passive image interferometry, *Geophys. J. Int.*, *168*, 1029–1033, doi:10.1111/j.1365-246X.2006.03284.x.

Wen, L. (2000), Intense seismic scattering near the Earth's core-mantle boundary beneath the Comoros hotspot, *Geophys. Res. Lett.*, *27*, 3627–3630, doi:10.1029/2000GL011831.

Wen, L. (2002), An SH hybrid method and shear velocity structures in the lowermost mantle beneath the central Pacific and South Atlantic Oceans, *J. Geophys. Res.*, *107*(B3), 2055, doi:10.1029/2001JB000499.

Wen, L. (2006), Localized temporal change of the earth's inner core boundary, *Science*, *314*, 967–970, doi:10.1126/science.1131692.

Young, R. P., and D. S. Collins (2001), Seismic studies of rock fracture at the Underground Research Laboratory, Canada, *Int. J. Rock Mech. Min. Sci.*, *38*, 787–799, doi:10.1016/S1365-1609(01)00043-0.

Yu, W., and L. Wen (2012), Deep-focus repeating earthquakes in the Fiji-Tonga subduction zone, *Bull. Seismol. Soc. Am.*, *102*, 1829–1849, doi:10.1785/0120110272.

Yue, H., and T. Lay (2011), Inversion of high-rate (1sps) GPS data for rupture process of the 11 March 2011 Tohoku earthquake (Mw 9.1), *Geophys. Res. Lett.*, *38*, L00G09, doi:10.1029/2011GL048700.

Zhang, J., X. Song, Y. Li, P. G. Richards, X. Sun, and F. Waldhauser (2005), Inner core differential motion confirmed by earthquake waveform doublets, *Science*, *309*, 1357–1360, doi:10.1126/science.1113193.

Zhang, J., P. G. Richards, and D. P. Schaff (2008), Wide-scale detection of earthquake waveform doublets and further evidence for inner core super-rotation, *Geophys. J. Int.*, *174*, 993–1006, doi:10.1111/j.1365-246X.2008.03856.x.

Zhao, P., and Z. Peng (2009), Depth extent of damage zones around the central Calaveras fault from waveform analysis of repeating earthquakes, *Geophys. J. Int.*, *179*, 1817–1830, doi:10.1111/j.1365-246X.2009.04385.x.